Acta Pharmaceutica Sinica B 2019;9(4):758–768

Chinese Pharmaceutical Association
Institute of Materia Medica, Chinese Academy of Medical Sciences

Acta Pharmaceutica Sinica B

www.elsevier.com/locate/apsb
www.sciencedirect.com

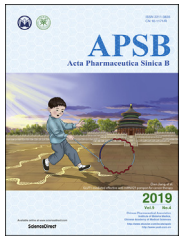

ORIGINAL ARTICLE

Regulation of microbiota–GLP1 axis by sennoside A in diet-induced obese mice

Jiamei Le[a,b], Xiaoying Zhang[c], Weiping Jia[d], Yong Zhang[e], Juntao Luo[c], Yongning Sun[b,f,*], Jianping Ye[c,d,e,*]

[a]*Shanghai Key Laboratory of Molecular Imaging, Shanghai University of Medicine and Health Sciences, Shanghai 201318, China*
[b]*Department of Traditional Chinese Medicine, Shanghai Jiaotong University Affiliated Sixth People's Hospital, Shanghai 200233, China*
[c]*Central Laboratory, Shanghai Jiaotong University Affiliated Sixth People's Hospital East, Shanghai 201306, China*
[d]*Diabetes Institute, Shanghai Jiaotong University Affiliated Sixth People's Hospital, Shanghai 200233, China*
[e]*Antioxidant and Gene Regulation Laboratory, Pennington Biomedical Research Center, LSU, Baton Rouge, LA 70808 USA*
[f]*Department of Cardiology, Shanghai Municipal Hospital of Traditional Chinese Medicine, Shanghai University of Traditional Chinese Medicine, Shanghai 200071, China*

Received 12 September 2018; received in revised form 3 December 2018; accepted 11 December 2018

KEY WORDS

Sennoside A;
Insulin sensitivity;
Mitochondria;
Gut microbiota;
Short chain fatty acids;
GLP1

Abstract Sennoside A (SA) is a bioactive component of Chinese herbal medicines with an activity of irritant laxative, which is often used in the treatment of constipation and obesity. However, its activity remains unknown in the regulation of insulin sensitivity. In this study, the impact of SA on insulin sensitivity was tested in high fat diet (HFD)-induced obese mice through dietary supplementation. At a dosage of 30 mg/kg/day, SA improved insulin sensitivity in the mice after 8-week treatment as indicated by HOMA-IR (homeostatic model assessment for insulin resistance) and glucose tolerance test (GTT). SA restored plasma level of glucagon-like peptide 1 (GLP1) by 90% and mRNA expression of *Glp1* by 80% in the large intestine of HFD mice. In the mechanism, SA restored the gut microbiota profile, short chain fatty acids (SCFAs), and mucosal structure in the colon. A mitochondrial stress was observed in the enterocytes of HFD mice with ATP elevation, structural damage, and complex dysfunction. The mitochondrial response was induced in enterocytes by the dietary fat as the same responses were induced by palmitic acid in the cell culture. The mitochondrial response was inhibited in HFD mice by SA treatment. These data suggest that SA may restore the function of microbiota–GLP1 axis to improve glucose metabolism in the obese mice.

*Corresponding authors.
E-mail addresses: Ynsun@sjtu.edu.cn (Yongning Sun), jianping.ye@pbrc.edu (Jianping Ye).

Peer review under responsibility of Institute of Materia Medica, Chinese Academy of Medical Sciences and Chinese Pharmaceutical Association.

https://doi.org/10.1016/j.apsb.2019.01.014

1. Introduction

Insulin resistance contributes to glucose disorder in the pathophysiology of type 2 diabetes in various conditions, including obesity and aging. Insulin resistance is a result of energy surplus with a feature of increased production of ATP by mitochondria[1]. Down-regulation of ATP production by decreasing energy intake or increasing energy discharge represents a promising approach in the treatment of insulin resistance, which are suggested by the effective therapies including the gastric bypass surgery and the sodium-glucose cotransporter 2 (SGLT2) inhibitor-based medicines[2,3].

Sennoside A (SA), a major active component of Chinese herb Rhizoma Rhei, is widely used as irritant laxative in clinical settings in China and other Asian countries. SA increases the large intestinal transit by induction of spontaneous colon contraction in a nerve-independent manner[4,5], which leads to a quick discharge of the intestinal content to cut down energy harvest from the diet. As a result, SA is a popular ingredient in variety of the weight-loss medicines or dietary supplements[6,7]. In the mechanism of action, SA was also reported to inhibit the enzyme activity of α-glucoamylase at a similar potency to acarbose[8]. Those studies suggest that SA may decrease energy harvest in the large intestine through acceleration of diet transit or inhibition of α-glucoamylase activity. However, the impact of SA on gut microbiota and intestine endocrinology has not been reported yet.

Microbiota regulates host energy metabolism through fermentation of dietary fibers in the large gut. Microbiota disorders increase the risk of insulin resistance, and type 2 diabetes[9,10]. The gut microbiota has been a target in the treatment of the metabolic diseases[11]. The gut microbiota catalyzes fermentation of dietary fibers to generate SCFAs including acetate, propionate and butyrate. SCFAs are energy sources for enterocytes in the production of ATP, glucose, cholesterol and triglyceride[12,13]. Butyrate is an important source of energy to the colon enterocytes, which involve in the maintenance of mucosal function of the colon[14,15]. SCFAs are reported to protect insulin sensitivity[16,17], improve glucose metabolism[18], and regulate immune functions[19], suggesting that SCFAs represent a class of beneficial products of gut microbiota in the regulation of host metabolism. It is unknown how the colon SCFA profile is regulated by SA. In this study, we investigated SA impact in the gut microbiota and SCFA in HFD mice.

In this study, the effect of SA on insulin sensitivity was examined in the HFD mice. SA impact in glucagon-like peptide 1 (GLP1), profiles of gut microbiota and SCFAs were determined in the large intestine to understand the mechanism of SA pharmacology activity. Mitochondrial function was examined in the colon enterocytes for the GLP1 response in the SA-treated mice. The data suggest that SA may regulate insulin action through an impact on microbiota–GLP1 axis.

2. Materials and methods

2.1. Chemicals and reagents

SA was obtained from the National Institute for Food and Drug Control (Beijing, China). The chemical standards included acetic acid, propionic acid, isobutyric acid, butyric acid, isovaleric acid, valeric acid as well as 2-methyl valerate. The purity of the above standards was all over 98% in HPLC. Other chemicals included fatty acid-free BSA, adenosine 5′-diphosphate sodium salt (ADP), carbonyl cyanide 4-(trifluoromethoxy) phenylhydrazone (FCCP), antimycin A, oligomycin, rotenone and succinic acid. Mitochondrial isolation buffer (MSHE+BSA) comprises 70 mmol/L sucrose, 210 mmol/L mannitol, 5 mmol/L HEPES, 1 mmol/L EGTA and 0.5% (*w*/*v*) fatty acid-free BSA (pH 7.2). Mitochondrial assay solution (MAS, 1 ×) was composed of 70 mmol/L sucrose, 220 mmol/L mannitol, 10 mmol/L KH_2PO_4, 5 mmol/L $MgCl_2$, 2 mmol/L HEPES, 1 mmol/L EGTA and 0.2% (*w*/*v*) fatty acid-free BSA, pH 7.2 at 37 °C. A 2–3 × stock of MAS was prepared for dilution of substrates, ADP and respiration reagents. Stocks of succinate (0.5 mol/L) and ADP (1 mol/L) were made in H_2O and adjusted to pH 7.2 with potassium hydroxide. Stocks of 10 m mol/L FCCP, 2 m mol/L rotenone, 5 mg/mL oligomycin and 40 m mol/L antimycin A were made in 95% ethanol. All chemicals were purchased from Sigma–Aldrich Co., Ltd. (Shanghai, China) unless stated separately. All reagents were stored at –20 °C except pyruvate, which was prepared fresh on the day of each experiment.

2.2. Animals

Eight-week old male C57BL/6 J mice (SPF grade) were obtained from Shanghai Slac Laboratory Animal Co., Ltd. (Shanghai, China). Animals were kept in an environment-controlled room (temperature: 20±2 °C, humidity: 60±5%, 12 h dark/light cycle). All animal experiments were conducted in accordance with the protocol approved by the Institutional Animal Care and Use Committee (IACUC) of Shanghai Jiaotong University (Shanghai, China). Normal control group (10 mice) was fed on a normal chow diet (NCD, 13.5% fat, Shanghai Slac Laboratory Animal Co., Ltd). A total of 20 mice were fed on HFD (60% kcal from fat, Research diets, # D12492) for 16 weeks to generate a diet-induced insulin-resistant model as previously described[20]. Insulin-resistant mice were divided randomly into 2 groups: HFD group (10 mice) and SA-treated HFD group (10 mice). SA was administrated at 30 mg/kg/day through drinking water. The treatment duration was 8 weeks, in which the body weight, food intake and water intake were monitored in the mice during the study (Fig. 1). Fecal moisture content was assessed by the ratio of fresh stool to dried stool. Fresh stool samples were collected at 0, 4 and 8 weeks of treatment and stored at –80 °C immediately for subsequent analysis. The fat pads were collected and weighted at 8 weeks of treatment when the mice were euthanized.

After 8 weeks of treatment, the animals were subject to tissue collection under anesthesia by intraperitoneal injection of pentobarbital (35 mg/kg). Blood was collected from the orbital plexus. Serum was isolated by centrifugation at 3000 × *g* at 4 °C for 10 min and stored at –80 °C until the biochemical assays. Following blood collection, the anesthetized mice were sacrificed by cervical dislocation. Visceral adipose tissues, livers and colons were collected from the animals and immediately weighed. The samples were flushed with phosphate-buffered saline (PBS, pH 7.4) and instantly frozen in liquid nitrogen and then stored at –80 °C until subsequent analysis.

2.3. GTT

GTT was performed in mice fasted for 16 h. Glucose (2 g/kg) was peritoneally injected and blood glucose was determined in the tail vein at 0, 15, 30, 60 and 120 min using a One Touch glucometer (ACCU-CHEK® Performa, Roche).

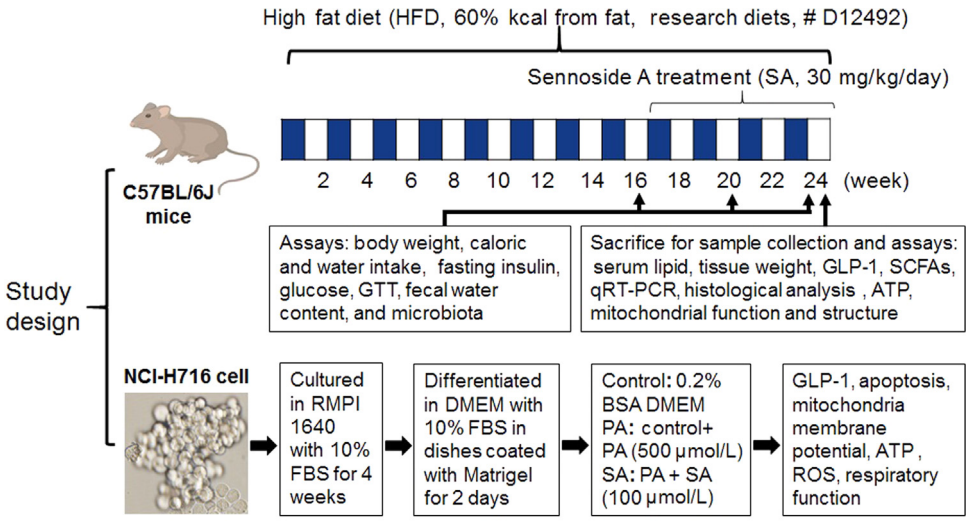

Figure 1 Study design.

2.4. *Fasting insulin and glucose assays*

Fasting insulin was determined in serum of mice fasted for 6 h with an ELISA kit (Thermo Fisher Scientific, Waltham, MA, USA). Fasting glucose was determined in serum of mice fasted for 16 h using a One Touch glucometer. According to the fasting insulin and glucose concentration, the insulin sensitivity index HOMA-IR was calculated according to Eq. (1) [21]:

$$\text{HOMA-IR} = \text{Fasting insulin}\,(\text{mU/L}) \times \text{Fasting glucose}\,(\text{mmol/L})/22.5 \quad (1)$$

2.5. *Histological analysis*

Colons were fixed in 10% phosphate-buffered formalin acetate at 4 °C overnight and embedded in paraffin wax. Paraffin sections (5 μm) were cut and mounted on glass slides for hematoxylin and eosin (H&E) staining as described[22]. The paraffin sections of colons were stained by Alcian blue-periodic acid-schiff (AB-PAS) staining according to the manufacturer's instructions (Solarbio, Beijing, China).

2.6. *Plasma GLP1 assay*

Blood GLP1 was determined with the GLP1 platinum ELISA kit (BMS2194, eBioscience, CA, USA). Mice were fasted for 12 h, and anesthetized by intraperitoneal injection of pentobarbital (35 mg/kg). Blood (300 μL) was collected in tube containing EDTA and DPP-IV inhibitor (1 mmol/L). The plasma was isolated by centrifugation at 3000 × *g* for 10 min at 4 °C and stored at −80 °C until test. DENLEY DRAGON Wellscan MK 3 software (Thermo, with Ascent software for Multiskan) was used in the analysis of GLP1 data.

2.7. *Microbiota assay*

The microbiota was tested in the fecal samples using the 16S ribosomal RNA protocol[23]. Total bacterial genomic DNA samples stored at −20 °C prior to further analysis were extracted using the Fast DNA SPIN extraction kits (MP Biomedicals, Santa Ana, CA, USA) following the manufacturer's instructions. The quantity and quality of extracted DNAs were measured using a NanoDrop ND-1000 spectrophotometer (Thermo Fisher Scientific, Waltham, MA, USA) and agarose gel electrophoresis, respectively.

Amplification of the bacterial 16 S rRNA genes V3–V4 region was performed using the forward primer 338 F (5′-ACTCCTACGG-GAGGCAGCA-3′) and the reverse primer 806 R (5′-GGAC-TACHVGGGTWTCTAAT-3′) in PCR. Sample-specific 7-bp barcodes were assembled into the primers for multiplex sequencing. The PCR components contained 5 μL of Q5 reaction buffer (5 ×), 5 μL of Q5 high-fidelity GC buffer (5 ×), 0.25 μL of Q5 high-fidelity DNA polymerase (5 U/μL), 2 μL (10 mmol/L) of dNTPs, 1 μL (10 μmol/L) of each forward and reverse primer, 2 μL of DNA Template, and 8.75 μL of ddH_2O. Thermal cycling was comprised of initial denaturation at 98 °C for 2 min, followed by 25 cycles consisting of denaturation at 98 °C for 15 s, annealing at 55 °C for 30 s, and extension at 72 °C for 30 s, with a final extension of 5 min at 72 °C. PCR amplicons were purified with Agencourt AMPure Beads (Beckman Coulter, Indianapolis, IN, USA) and quantified using the PicoGreen dsDNA Assay Kit (Invitrogen, Carlsbad, CA, USA). After the individual quantification step, amplicons were pooled in equal amounts, and pair-end 2 × 300 bp sequencing was performed using the Illlumina MiSeq platform with MiSeq reagent kit v3 at Shanghai Personal Biotechnology Co., Ltd. (Shanghai, China).

The Quantitative Insights Into Microbial Ecology (QIIME, v1.8.0) pipeline was employed to process the sequencing data in microbiota analysis. Briefly, raw sequencing reads with exact matches to the barcodes were assigned to respective samples and identified as valid sequences. The low-quality sequences were excluded if the following criteria were not matched: (1) sequences that had a length of < 150 bp, (2) sequences that had average Phred scores of < 20, (3) sequences that contained ambiguous bases, and (4) sequences that contained mononucleotide repeats of > 8 bp. Paired-end reads were incorporated using FLASH. After chimera detection, the remaining high-quality sequences were clustered into operational taxonomic units (OTUs) at 97% sequence identity by UCLUST. A representative sequence was selected from each OTU using default parameters. OTU taxonomic classification was conducted by BLAST searching the representative sequences set against the Greengenes Database using the best hit. OTU abundance data were then used for the calculation of ACE (abundance coverage-based estimator of species richness) index and for rarefaction estimates *via* QIIME. Taxonomical

assignments of representative sequences were determined using the RDP classifier with a bootstrap cutoff of 50%.

2.8. SCFA assay

Freeze-dried fecal samples (0.1 g) were reconstituted in 0.4 mL distilled water followed by centrifugation (5000 rpm, 20 min at 4 °C). The supernatant was acidified with a 1/5 volume of 50% H_2SO_4 and 1/2 volume of dilution internal standard solution (50 μg/mL), and then extracted with ethyl ether. The concentrations of SCFAs including acetic acid, propionic acid, isobutyric acid, butyric acid, valeric acid, and isovaleric acid were determined in the organic phase using Gas chromatography (GC-2010, Shimadzu Cooperation, Kyoto, Japan), in which 2-methyl valerate was the internal standard solution. It was equipped with a flame ionization detector and an All-tech capillary column (AT-WAX, 30 m × 0.25 mm × 0.25 μm, Alltech company, ME, USA) operated in the split-less mode. The helium carrier flow was 37.0 cm/s under a column head pressure of 68.0 kPa. The oven temperature was initially 100 °C for 1 min, increased to 170 °C at a rate of 5 °C/min , gradually increased to 230 °C at a rate of 30 °C/min, and maintained for 2 min. The injector and detector temperatures were set at 220 °C and 250 °C, respectively.

2.9. Quantitative real-time PCR (qRT-PCR)

Total RNA was extracted using the TRIzol RNA isolation reagent (Invitrogen, Carlsbad, CA, USA). Reverse transcription of 500 ng RNA was carried out according to the instructions of Prime Script™ 1st strand cDNA synthesis kit (TaKaRa, Japan). The qRT-PCR reaction was conducted in 20 μL (SYBRH Premix Ex TaqTM, TaKaRa Japan) using the applied primer sequences listed in Supporting information Table S1. The result was normalized against *Gapdh* mRNA signal.

2.10. Mitochondria and ATP assays

Mitochondria were isolated from colons by differential centrifugation, and mitochondrial oxygen consumption rates (OCR) were measured using an XF24 Analyzer (Seahorse Bioscience Inc., North Billerica, MA, USA)[24]. The mitochondrial complex assay was performed with 5 μg mitochondria per well, 10 mmol/L pyruvate, 2 mmol/L malate and 4 mmol/L FCCP. The inhibitors included rotenone (2 mmol/L), succinate (10 mmol/L), antimycin A (4 mmol/L final), and ascorbate plus 1 mmol/L *N*,*N*,*N*^{9},*N*^{9}-tetramethyl-*p*-phenylenediamine (TMPD, 10 mmol/L and 100 mmol/L, respectively). ATP level was determined in fresh tissues with the EnzyLightTM ATP assay kit (EATP-100, BioAssay Systems, Northern CA, USA). DENLEY DRAGON Wellscan MK 3 software (Thermo, with Ascent software for Multiskan) was used in analysis of insulin, GLP1 and ATP data.

2.11. Ultrastructure of mitochondria

The colon tissues were rapidly sliced on ice and fixed in 4% glutaraldehyde solution. Then, specimen of electron microscope was made through fixing in 1% osmium acid, dehydration of gradient ethanol, epoxy resin embedding and ultrathin section. The mitochondrial ultrastructure of mice liver and colon were observed with a biology transmission electron microscopy (Tecnai G2 Spirit Biotwin/*Tecnai G2 spirit Biotwin, 120 kV, Hillsboro, OR, USA).

2.12. Mitochondrial stress responses in cellular model

The L-cell line, NCI-H716 cells (CCL-251™, ATCC), was purchased from the Cell Bank of the China Science Academy (Shanghai, China). The cells were cultured in RMPI 1640 medium with 10% fetal bovine serum in the absence of mycoplasma contamination. Differentiation into L-cells was induced by growing cells in dishes coated with Matrigel (Becton Dickinson, Bedford, MA, USA). In the assay, the cells were maintained in DMEM medium supplemented with 0.2% bovine serum albumin (BSA). Mitochondrial stress responses and cell apoptosis were induced by treatment of the cells with palmitic acid (PA) for 24 h at a final concentration of 500 μmol/L. SA was used at a final concentration of 100 μmol/L to block the lipotoxicity.

Apoptosis was determined with an annexin V-FITC apoptosis detection kit (Dojindo, Shanghai, China) and cell necrosis was determined with propidium iodide (PI) staining using the flow cytometry. Mitochondrial membrane potential was determined with JC-1 fluorescent dye (Beyotime, Shanghai, China) in combination with the flow cytometry. OCR was determined with the Seahorse technology. ATP was determined in the cell lysate using the EnzyLightTM ATP assay kit described above. For GLP1 secretion assay, the supernatants were collected and GLP1 levels were measured with a GLP1 platinum ELISA kit after incubating with the Krebs-Ringer bicarbonate buffer (128.8 mmol/L NaCl, 4.8 mmol/L KCl, 1.2 mmol/L KH_2PO_4, 1.2 mmol/L $MgSO_4$, 2.5 mmol/L $CaCl_2$, 5 mmol/L $NaHCO_3$, 10 mmol/L HEPES, and 0.2% BSA, pH 7.4). The average fluorescent intensities (to correct for differences in cell number) were quantified using ImagePro Plus version 5.0 imaging software (Media Cybernetics, Rockville, MD, USA).

2.13. Data analysis

Results were expressed as the mean ± standard deviation (SD). The statistical analyses were conducted using two-way ANOVA and Student's *t*-test. A P value < 0.05 is considered to be statistically significant.

3. Results

3.1. Inhibition of obesity and hyperlipidemia by SA

SA is an ingredient in the herbal medicines or dietary supplements for weight control on its laxative activity[6,7]. However, the SA pharmacology activity has not been carefully examined in an animal model of obesity. We tested the SA activity in diet-induced obese model, which was established in C57BL/6 mice with HFD feeding for 16 weeks. SA was administrated into the mice through dietary supplementation for 8 weeks. Body weight was monitored at the start, 4 and 8 weeks of the treatment. An increase in body weight was observed in the untreated group. However, the increase was significantly less in the SA-treated group (Fig. 2A). The significance was also observed in the data analysis with two-way ANOVA (Supporting information Table S2). The difference was observed at 4 and 8 weeks without a reduction in calorie intake, which was not decreased in the treated mice (Fig. 2B). A less gain in fat tissue was observed in the lower weight of epididymal and prerenal fat pads in the treated mice (Fig. 2C). The hyperlipidemia was improved in the treated group as well for the reduction in the low density lipoprotein C, total cholesterol, and total triglyceride

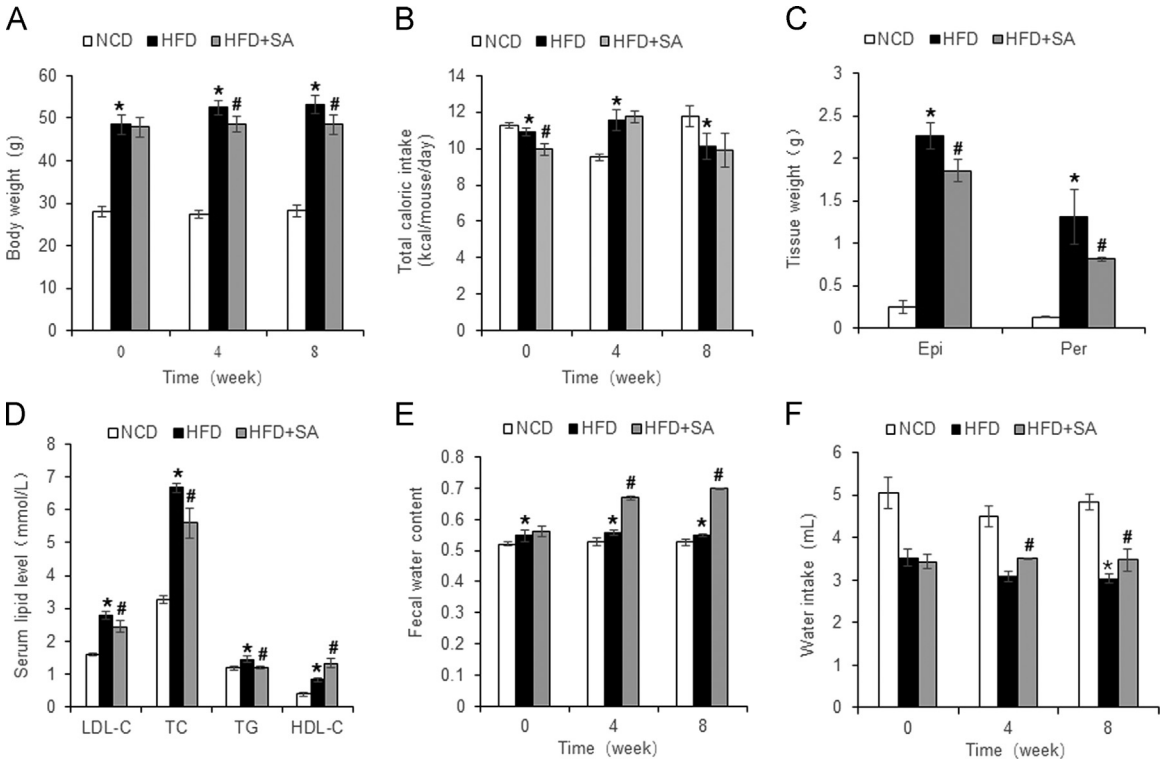

Figure 2 Inhibition of obesity and hyperlipidemia by SA. (A) Body weight at 0, 4 and 8 weeks of treatment. (B) Calorie intake. (C) Tissue weight of perirenal fat and epididymal fat pads after 8 weeks of treatment. (D) Serum lipid levels after 8 weeks of treatment. (E) Fecal moisture content. (F) Water intake at 0, 4 and 8 weeks of treatment. The SA treatment was administrated for 8 weeks in DIO mice after 16 weeks on high-fat diet. Data are presented as the mean ± SD ($n = 10$). $^{*}P < 0.05$, HFD *versus* NCD; $^{\#}P < 0.05$, HFD+SA *versus* HFD.

in the blood. High density lipoprotein C was increased by the treatment (Fig. 2D). The improvement in body weight, fat mass and hyperlipidemia suggest that SA is able to attenuate the energy surplus status in the obese mice. The mechanism is likely due to loss of energy in feces from the laxative activity of SA. In support, water content was increased in the feces of treated mice at 4 and 8 weeks (Fig. 2E), suggesting a less stay of feces in the colon. The fecal water loss provides a basis for the increased water intake in the treated mice (Fig. 2F). The diet-induced obesity (DIO) model was successfully established in the mice with HFD feeding as indicated by the body weight, fat mass and hyperlipidemia over the chow diet-fed mice (Fig. 2A–D).

3.2. *Improvement of insulin sensitivity by SA*

SA is known to reduce obesity, but its impact on insulin sensitivity remains to be tested. Insulin sensitivity was examined in DIO mice at 4 and 8 weeks into SA-treatment. Fasting blood glucose was decreased at both time points, but the reduction in fasting insulin occurred only at 8 weeks (Fig. 3A and B). Insulin sensitivity index of HOMA-IR was improved at both time points (Fig. 3C). The change was also observed in analysis with two-way ANOVA (Table S2). Intra peritoneal glucose tolerance test (ipGTT) was conducted to determine the SA activity. An improvement was observed at 4 and 8 weeks as indicated by the reduction in area under curve (Fig. 3D–F). At the molecular level, insulin sensitivity was observed in liver for a reduction in the gluconeogenic genes (G6Pase and PEPCK) (Fig. 3G and H). This group of data suggests that SA is able to improve insulin sensitivity in DIO mice. Insulin resistance was successfully established in the model as indicated by the increased value in HOMA-IR and GTT over the normal control mice (Fig. 3A–H).

3.3. *Restoration of GLP1 and Gpr43 by SA*

GLP1 is a gut hormone secreted by L-cells in the mucosa of large intestine. GLP1 analogues are widely used in the treatment of type 2 diabetic patients worldwide. It is unknown if GLP1 secretion and expression are regulated by SA. To address the issue, GLP1 protein was examined in the serum and mRNA was determined in the colon. Plasma GLP1 was reduced by 90% in the DIO mice and the 80% reduction was normalized by SA treatment (Fig. 4A). mRNA of *Glp1* was determined by examining glucagon gene in the colon, and a 80% reduction was detected in DIO mice. 90% reduction was corrected by SA (Fig. 4B), which provides a mechanism for the restoration of GLP1 protein in the serum. GPR43 and GPR41 are receptors of SCFAs in the enterocytes of intestine to mediate induction of GLP1 secretion by L-cells[25]. Their expression was reduced in DIO mice, and the reduction was partially restored by SA (Fig. 4C and D). The data suggests that SA may restore L-cell function in the large intestine for GLP1 secretion.

3.4. *Regulation of SCFAs and gut microbiota by SA*

SCFAs are produced in the large intestine by microbiota in fermentation of dietary fibers. Among SCFAs, butyric acid was reported to improve insulin sensitivity[16] and to induce GLP1 expression in L-cells[26]. It is unknown if SCFAs and gut microbiota are changed by SA. To address the issue, butyric acid was examined together with other 5 types of SCFAs (acetic acid,

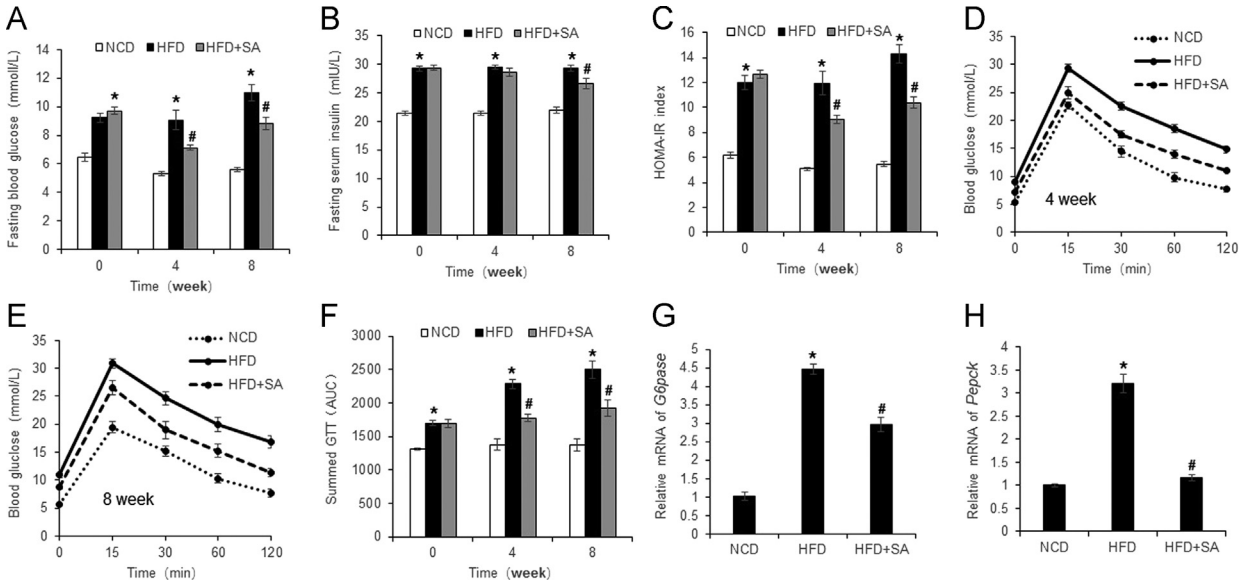

Figure 3 Improvement of insulin sensitivity by SA. (A) Fasting blood glucose. (B) Fasting plasma insulin. (C) HOMA-IR. (D) GTT at 4 weeks of SA treatment. GTT was performed by intraperitoneal injection of glucose (2 g/kg body weight). (E) GTT at 8 weeks of SA treatment. (F) Area under the curve of GTT assays. (G) mRNA of *G6Pase* in liver tissue at 8 weeks of SA treatment. (H) mRNA of *Pepck* in liver tissue at 8 weeks of SA treatment. Data are presented as the mean ± SD ($n = 10$). $^{*}P < 0.05$, HFD *versus* NCD; $^{\#}P < 0.05$, HFD+SA *versus* HFD.

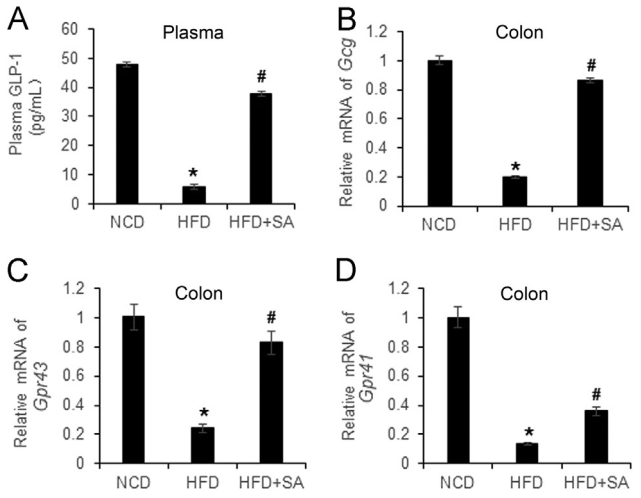

Figure 4 Restoration of GLP1, GPR43 and GPR41 in large gut by SA. (A) Plasma GLP1. (B) mRNA expression of *Gcg* in the colon tissue. (C) mRNA expression of *Gpr43* in the colon tissue. (D) mRNA of *Gpr41* expression in the colon tissue. Data are presented as the mean ± SD ($n = 3$). $^{*}P < 0.05$, HFD *versus* NCD; $^{\#}P < 0.05$, HFD+SA *versus* HFD.

propionic acid, isobutyric acid, valeric acid, and isovaleric acid) in the feces of mice to understand the effect of SA. Among SCFAs, butyric, acetic and propionic acids were most abundant with concentrations between 140–260 μg/mL in the normal control mice (Fig. 5A–C). The other 3 types of SCFAs had 3–5-fold less in concentrations at 20–35 μg/mL (Fig. 5D–F). Butyric acid exhibited the most reduction in DIO mice although all of SCFAs were significantly reduced (Fig. 5A–F). The reduction in most of SCFAs was partially restored by SA.

To investigate the impact of SA in the gut microbiota, the fecal samples were analyzed for microbiota using the 16S ribosomal RNA protocol[23]. Microbiota diversity (richness and evenness) was determined in the mice. An increase in diversity was observed with the ACE index in HFD mice over NCD mice (Fig. 5G). The increase was suppressed by SA. At the phylum level, Firmicutes and Bacteroidetes are the most abundant bacteria in the gut microbiota. Firmicutes was increased, and Bacteroidetes was decreased by HFD (Fig. 5H and I). The up-regulated Firmicutes was significantly reduced by SA, but the down-regulated Bacteroidetes was not significantly changed. The ratio of Firmicutes to Bacteroidetes, a widely used marker of gut dysbiosis[27], was increased by 10-fold in HFD mice, and the increase was eliminated by SA (Fig. 5J). At the genus level, the relative abundance of Clostridiales.g, Desulfovibrionaceae.g, and Oscillospira was increased by HFD, and the increase was eliminated by SA (Fig. 5K–M). In contrast, abundance of *Allobaculum* (a genus of butyrate-producing bacteria)[28] was continuously decreased by HFD in the study, and the reduction was partially prevented by SA (Fig. 5N). Abundance of *Allobaculum* was also reduced in NCD mice at 8-week time point in the study with unknown reasons. The data suggests that SA is able to correct dysbiosis in the gut of obese mice.

3.5. *Restoration of colon mucosa structure by SA*

In the study of gastric bypass effect on insulin sensitivity, we established a mouse model of Roux-en-Y bypass surgery (RYGB)[29,30]. In the analysis of surgery effect on intestine, we found that the total length of small intestine was reduced in DIO mice over the normal control mice, suggesting that atrophy was induced in the intestine by HFD. The reduction in GLP1 secretion and expression may reflect the atrophy. To test the possibility, the colon was examined for structural integrity under the microscope. An impaired structure was observed in the colon mucosa of DIO mice for de-attachment of epithelial cells and reduced mucosa content in the colonic wall (Fig. 6). These defects were corrected partially by SA in the colonic wall, suggesting that SA may protect the structure of colon wall.

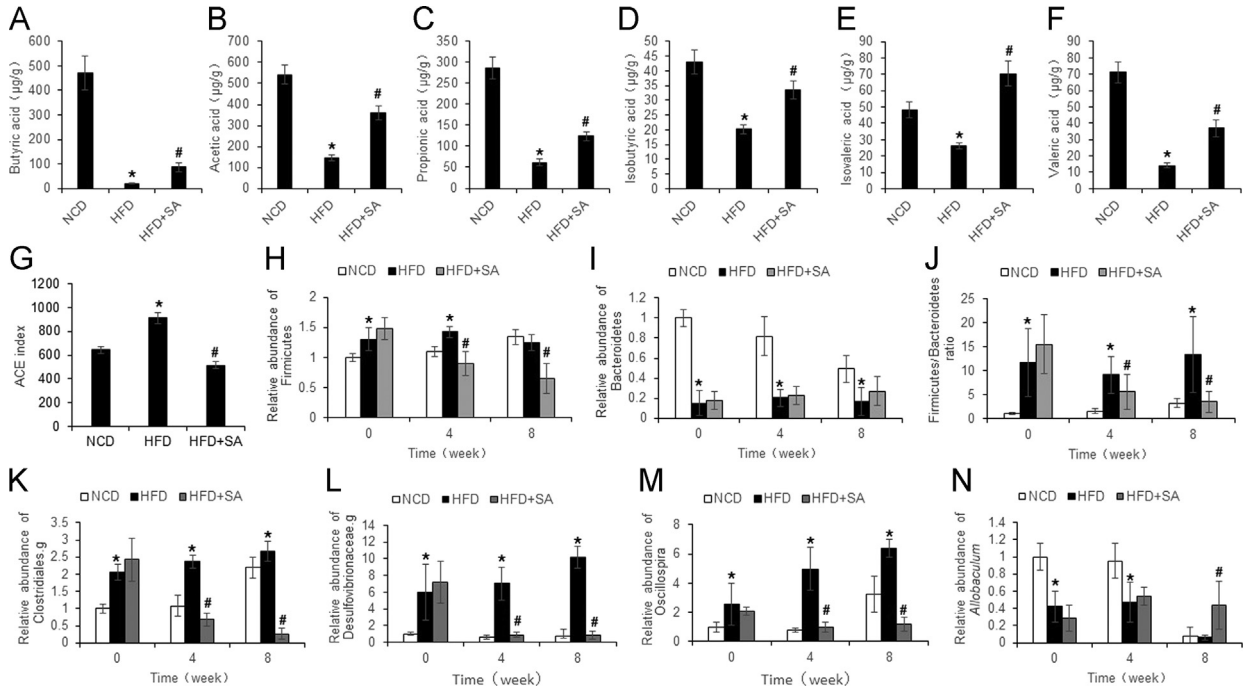

Figure 5 Regulation of SCFAs and gut microbiota by SA. (A)–(F) The concentration of acetic acid, propionic acid, isobutyric acid, butyric acid, isovaleric acid and valeric acid in feces of HFD mice after 8 weeks of SA treatment. (G) Bacteria diversity in feces as indicated by ACE richness. (H)–(I) The abundance of Firmicutes and Bacteroidetes. (J) The Firmicutes/Bacteroidetes ratio. (K)–(N) The abundances of Clostridiales. g, Desulfovibrionaceae.g, Ruminococcaceae.g and *Allobaculum*. Data are presented as the mean ± SD ($n = 10$). $^{*}P < 0.05$, HFD *versus* NCD; $^{\#}P < 0.05$, HFD+SA *versus* HFD.

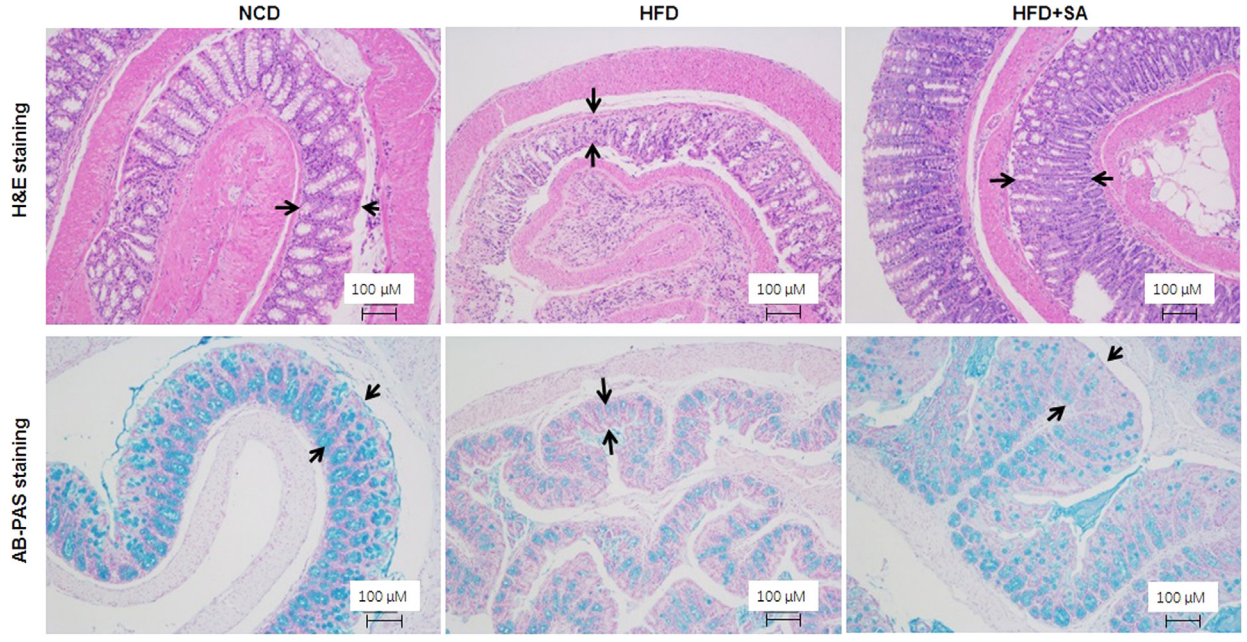

Figure 6 Protection of colon mucosa structure by SA. Colon tissue histology was examined in H&E and AB-PAS staining. The images of representative fields were taken from the colon tissue slides (100 ×, scale bar = 100 μm).

3.6. *Protection of enterocyte mitochondria by SA*

To understand the mechanism of SA activity, mitochondria were examined in the colon enterocytes. Energy surplus leads to ATP over production in DIO mice[24,31], which may generate an impact in mitochondria. To test the possibility, mitochondrial structure and function were examined in the colon enterocytes. A structure damage was observed in the DIO mice with mitochondrial swelling, membrane rapture and loss of crista (Fig. 7A). The structure defects were corrected by SA.

The function of mitochondria was examined by examination of ATP level in the fresh tissue homogenization and mitochondrial

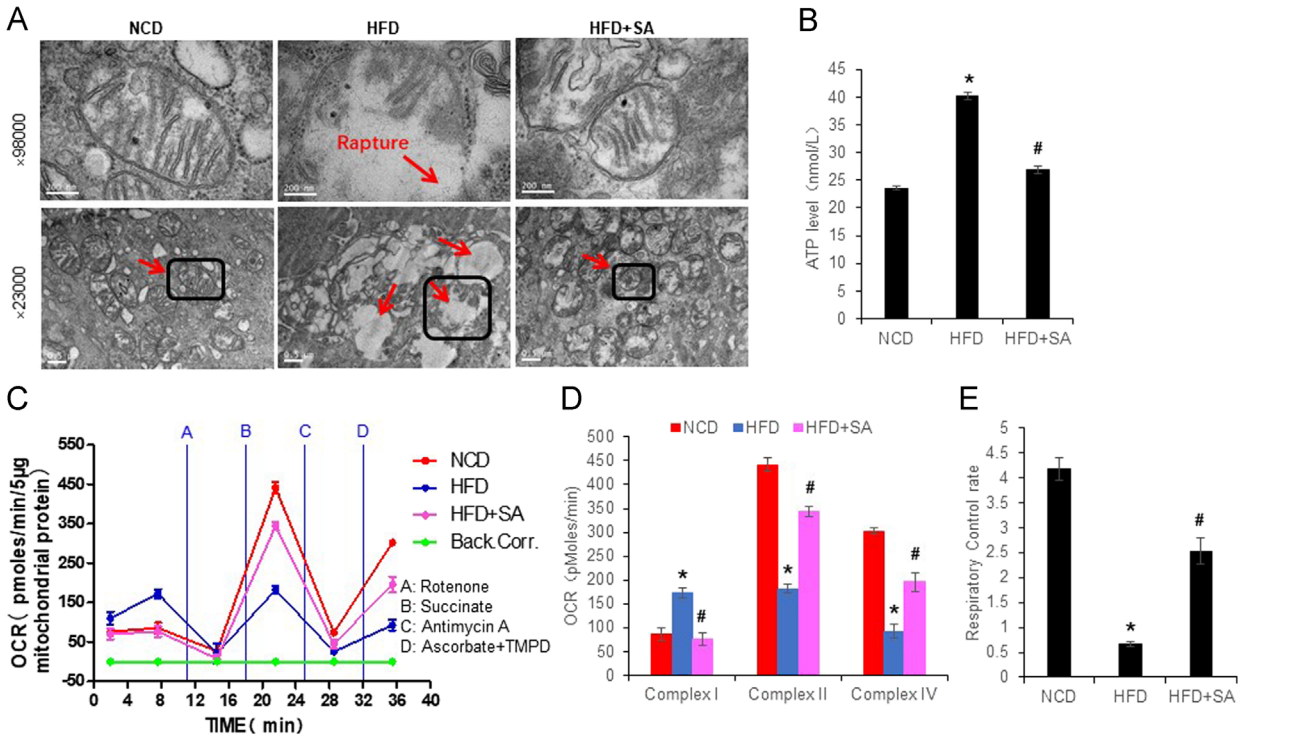

Figure 7 Improvement of mitochondrial structure and function by SA in colon enterocytes. (A) Mitochondrial structure under a transmission electron microscope. The images of 98,000 × were derived from the mitochondria in the square of image of 23,000 × . (B) ATP level in the fresh colon tissue. (C) The complex activities of mitochondria. The complex activity was determined with the oxygen consumption rate (OCR) in response to the complex inhibitors in mitochondria isolated from the fresh colon tissue. The order of inhibitor injection was rotenone, succinate, antimycin A, and ascorbate plus *N*,*N*,*N*^{9},*N*^{9}-tetramethyl-*p*-phenylenediamine (TMPD). (D) Mean value of maximal OCR in the complex assay. (E) Mitochondrial function as indicated by respiration control rate. Data are presented as the mean ± SD ($n = 6$). $^*P < 0.05$, HFD *versus* NCD; $^\#P < 0.05$, HFD+SA *versus* HFD.

complex activity. An elevation was observed in ATP level of the colon tissue of DIO mice (Fig. 7B). The elevation was attenuated by SA treatment. The complex activities of respiration chain were examined using the isolated mitochondria with the Seahorse technology. The complex I activity was increased; the complex II and IV activities were decreased in DIO mice over the control mice (Fig. 7C and D). The alteration in complex I was completely corrected, partially corrected in the complexes II and IV by SA. The respiratory control rate of mitochondria was dramatically decreased in DIO mice, and partially restored by SA (Fig. 7E). These data suggest that mitochondrial damage was induced in the colon enterocytes by HFD, and the damage was attenuated by SA treatment.

3.7. *Induction of L-cell stress response by dietary fat*

The colon enterocytes use the short chain fatty acids (butyric acid) in the fuel consumption for production of ATP by mitochondria. However, this pattern of fuel consumption is interrupted by the dietary fat of HFD and the SCFA reduction in the large intestine. The change may lead to the stress response in mitochondria of the enterocytes of DIO mice for the reduction in GLP1 secretion. To test this potential mechanism, palmitic acid (PA) was used to treat L-cells derived from the epithelial cell line NCI-H716 in the cell culture, which is a cellular model to mimic the condition in DIO mice. GLP1 secretion and mRNA expression were significantly inhibited in the model by PA treatment (Fig. 8A and B). In the mitochondrial responses, ATP level was increased, membrane potential and oxygen consumption were significantly decreased by the treatment (Fig. 8C–E). Cell apoptosis was induced as well by the treatment (Fig. 8F). This group of data suggests that the L-cells suffer a stress response to the fuel supply by the long chain fatty acids, which supports the potential mechanism of enterocyte damage and GLP1 reduction in DIO mice.

4. Discussion

This study provides evidence that SA is able to improve insulin sensitivity in obese mice. Natural products are resources of drug candidates in the control of metabolism[32,33]. SA is a single bioactive compound originally identified in the Chinese herb Rhizoma Rhei (RR). In current study, SA improved insulin sensitivity in DIO mice for the reduction in HOMA-IR and improvement in GTT. The effect was associated with a body weight reduction, which may reflect less energy absorption in the gut due to the laxative effect. Weight loss contributes to insulin sensitization through attenuation of energy surplus in the body. Current study suggests that restoration of GLP1 may contribute the weight loss and insulin sensitization in SA-treated mice. GLP1 protein was increased in the blood and its mRNA was increased in the colon tissue of SA-treated mice, which represent a new activity of SA in the regulation of glucose metabolism.

HFD induced mucosal damage in the large intestine of DIO mice, which was attenuated by SA. GLP1 is secreted by L-cells in the mucosa of large intestine upon stimulation by the nutrients. The gene expression was decreased in the intestine of DIO mice in this study and other study[34]. The mechanism is unknown for the reduction.

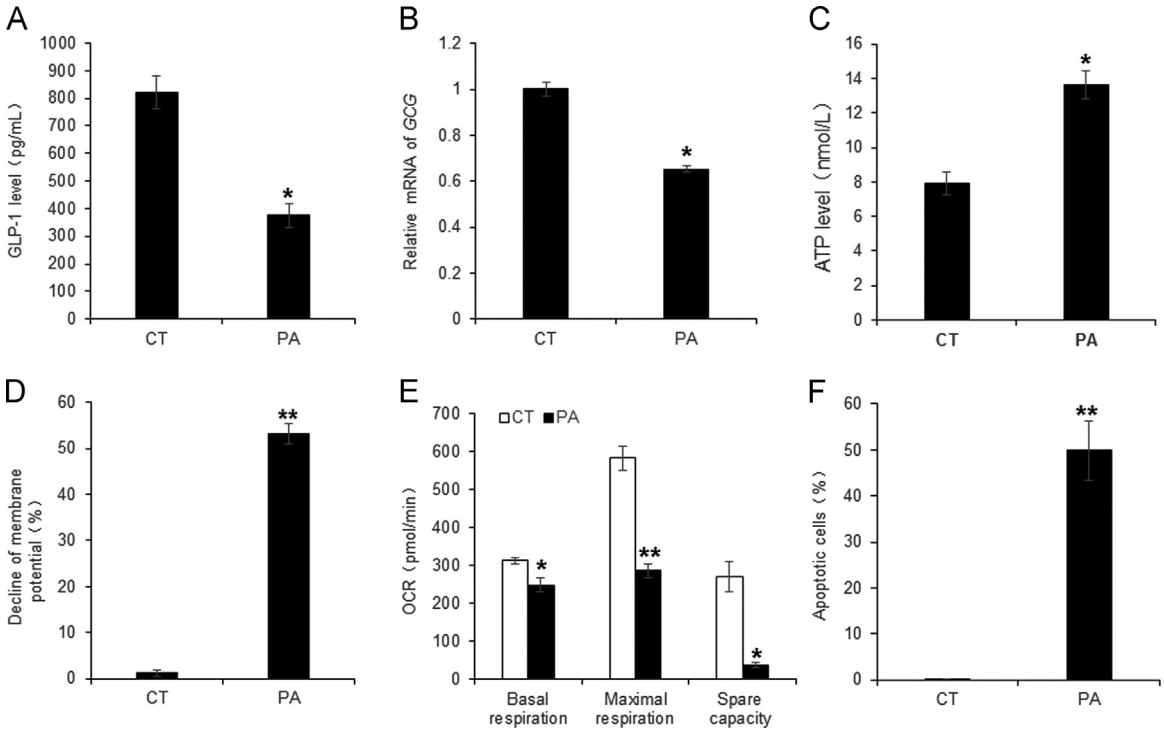

Figure 8 Inhibition of L cell activity by PA. Palmitic acid (PA) was used to represent the dietary fat in the induction of mitochondrial responses in L-cells of the intestine epithelial cell line NCI-H716. (A) GLP1 levels in supernatant of PA-treated L-cells. (B) mRNA expression of *GCG* in PA-treated L-cells. (C) ATP elevation in PA-treated L-cells. (D) Mitochondrial membrane potential in PA-treated L-cells. (E) Reduced OCR in PA-treated L-cells. (F) Increased apoptosis in PA-treated L-cells. Data are presented as the mean ± SD ($n = 3$). $^{*}P < 0.05$, $^{**}P < 0.001$ PA *versus* blank control.

Some studies suggest that the reduction is due to L-cell dysfunction instead of a reduction in L-cell number[35–37]. However, mechanism of the dysfunction remains unknown. Current study suggests that the mitochondrial damage contributes to the cell dysfunction. In histology, the DIO mice exhibited a structural damage in the colon mucosa, which was observed with a reduction in thickness of mucosa, lack of mucus content in the mucosal cells, and detachment of epithelial cells in the mucosa surface. In support, mRNA expression of *Gpr43* and *Gpr41* genes was significantly reduced in the intestine epithelial cells of colon. The tissue damages were prevented by SA in DIO mice, suggesting that HFD may cause a mucosa damage in the colon of DIO mice to inhibit the L-cell function. SA was able to correct the tissue damages.

HFD induced mitochondrial dysfunction in the colon enterocytes of DIO mice, which was corrected by SA. To understand the mechanism of tissue damage, we investigated mitochondria in the enterocytes of colon. ATP level was examined in the colon tissue and an increase was detected in the DIO mice, suggesting an over production of ATP in the tissue due to "mitochondrial overheating"[38]. To explore the mechanism, L-cells were treated with PA in the cell culture to mimic the effect of HFD on the gut epithelial-cells. Intracellular ATP was induced by the PA treatment, which was companied by an elevation of ROS and damage of mitochondrial function. Consistently, cell apoptosis was increased in the L-cells with PA treatment. Mitochondria are able to generate more reactive oxygen species (ROS) upon ATP over production following an increase in substrate influx, which is known as "mitoflash" in myocytes[39,40]. The ROS response is activated to decrease ATP production through a reduction in the membrane potential of mitochondria in mitoflash. The ROS response was observed in the DIO mice with the increase in the complex I activity, a major source of ROS in mitochondria. ROS is able to induce the damage of mitochondrial structure, such as loss of crista, mitochondrial swelling and membrane rupture, which were observed in the intestine tissue of DIO mice. ROS impairs mitochondria through oxidation of lipids and proteins in the mitochondrial membrane[39,41]. The mitochondrial damage was corrected by SA likely through reduction of exposure of enterocytes to the dietary fat following the laxative effect.

The data suggests that SA reduced ATP elevation in the large intestine tissue. The ATP level was elevated in the intestine tissue of DIO mice, suggesting a result of fuel switch from SCFAs to the long chain fatty acids. Enterocytes of large intestine normally use SCFAs in fuel consumption in the large intestine. However, the fuel supply is switch to the long chain fatty acids in the HFD of DIO mice. The switch induced ATP production and mitochondrial damage as a result of the toxicity of the long chain fatty acids. The damage likely happened in some of the cells, which was not sufficient to bring down the elevated level of ATP in the colon tissue. In addition to production of ATP, mitochondria also consume ATP to preserve the membrane potential under stress conditions[42]. The mitochondrial damage may contribute to the ATP elevation through a decrease in ATP consumption in the DIO mice. SA reduced the ATP elevation, which provides a mechanism for the SA activity in the protection of colon enterocytes in DIO mice.

Restoration of SCFAs may contribute to the SA activity in the regulation of mitochondrial function. Dysbiosis was observed in the DIO mice for an increase in the gut microbiota diversity and the elevated ratio of Firmicutes/Bacteroidetes, which is consistent with the reports in literature[27]. The dysbiosis led to a reduction in SCFAs in the large intestine. Six SCFAs were examined in this study, and all of them were decreased in abundance in the large gut of DIO mice. The dysbiosis was partially corrected, and SCFA levels were mostly restored by SA in the DIO mice. As a major

form of SCFAs, butyrate was restored in abundance by SA. Relative to the long chain fatty acids, butyrate generates much less ROS in the production of ATP in mitochondria. Substitution of long chain fatty acids with butyrate should bring down the ROS production in the enterocytes in the DIO mice. In support, the abundance of butyrate-producing bacteria is positively associated with the antioxidant capacity in the gut of type 2 diabetes patients[43]. In addition, butyrate is able to stimulate GLP1 secretion in L-cells through activation of the G-protein-coupled receptor (GPR43 or GPR41)[25]. These lines of evidence suggest that the alteration in microbiota and SCFAs may contribute to the SA activity in the regulation of GLP1 secretion. However, this possibility remains to be further tested using a germ-free system.

The SA dosage was 30 mg/kg/day in this study, which is far below LD_{50} (1414 mg/kg/day) of SA in mouse. The dosage was selected according to the safe and effective dosages (12.5–200 mg/kg) in a study of the laxative[44]. In human, the equivalent dosage will be 5 mg/kg/day according to the dosage in current study as the mouse metabolic rate is 6 times of human.

There are several limitations in this study. The study was conducted only in DIO model. The SA effect remains to be tested in other animal models and even obese patients. A change in electrolyte levels and water balance may contribute to the weight loss in SA-treated mice. The possibility was not tested in this study. The study suggests that SA protects L-cells through restoration of SCFA profile in the large intestine. However, the possibility needs to be examined by excluding a direct effect of SA on L-cells.

5. Conclusions

The study demonstrated that oral administration of sennoside A increased glucose metabolism and insulin sensitivity in DIO mice. The activity was observed with restoration of circulation GLP1, colon *Glp1* expression and protection of L-cells in the colon mucosa by SA. The SA effect was associated with restoration of the mitochondrial function in the large intestine enterocytes of DIO mice following correction of gut microbiota and SCFAs. The data suggests that restoration of GLP1 may contribute to the SA activity in the regulation of insulin sensitivity.

Acknowledgments

The project was supported by the National Natural Science Foundation of China (81874377) to Yongning Sun and the National Natural Science Foundation of China (81220108006) to Weiping Jia and Jianping Ye. This study was also supported by the internal fund of the Shanghai Jiaotong University Affiliated Sixth People's Hospital East (Shanghai, China) to Jianping Ye and Yongning Sun.

Appendix A. Supporting information

Supporting data associated with this article can be found in the online version at https://doi.org/10.1016/j.apsb.2019.01.014.

References

1. Ye J. Mechanisms of insulin resistance in obesity. *Front Med* 2013;**7**:14–24.
2. Yin DP, Gao Q, Ma LL, Yan W, Williams PE, McGuinness OP, et al. Assessment of different bariatric surgeries in the treatment of obesity and insulin resistance in mice. *Ann Surg* 2011;**254**:73–82.
3. Abdul-Ghani MA, DeFronzo RA. Inhibition of renal glucose reabsorption: a novel strategy for achieving glucose control in type 2 diabetes mellitus. *Endocr Pract* 2008;**14**:782–90.
4. Kobayashi M, Yamaguchi T, Odaka T, Nakamura T, Tsuchiya S, Yokosuka O, et al. Regionally differential effects of sennoside A on spontaneous contractions of colon in mice. *Basic Clin Pharmacol Toxicol* 2007;**101**:121–6.
5. Rumsey RD, Squires PE, Read NW. *In vitro* effects of sennoside on contractile activity and fluid flow in the perfused large intestine of the rat. *Pharmacology* 1993;**47 suppl 1**:S32–9.
6. Kim HJ, Lee JH, Park HJ, Cho SH, Cho S, Kim WS. Monitoring of 29 weight loss compounds in foods and dietary supplements by LC–MS/MS. *Food Addit Contam Part A Chem Anal Control Expo Risk Assess* 2014;**31**:777–83.
7. Greenway FL, Liu Z, Martin CK, Kai-yuan W, Nofziger J, Rood JC, et al. Safety and efficacy of NT, an herbal supplement, in treating human obesity. *Int J Obes* 2006;**30**:1737–41.
8. Choi SB, Ko BS, Park SK, Jang JS, Park S. Insulin sensitizing and α-glucoamylase inhibitory action of sennosides, rheins and rhaponticin in Rhei Rhizoma. *Life Sci* 2006;**78**:934–42.
9. Vrieze A, van Nood E, Holleman F, Salojarvi J, Kootte RS, Bartelsman JF, et al. Transfer of intestinal microbiota from lean donors increases insulin sensitivity in individuals with metabolic syndrome. *Gastroenterology* 2012;**143**:913–6. e7.
10. Vijay-Kumar M, Aitken JD, Carvalho FA, Cullender TC, Mwangi S, Srinivasan S, et al. Metabolic syndrome and altered gut microbiota in mice lacking Toll-like receptor 5. *Science* 2010;**328**:228–31.
11. Delzenne NM, Neyrinck AM, Backhed F, Cani PD. Targeting gut microbiota in obesity: effects of prebiotics and probiotics. *Nat Rev Endocrinol* 2011;**7**:639–46.
12. Topping DL, Clifton PM. Short-chain fatty acids and human colonic function: roles of resistant starch and nonstarch polysaccharides. *Physiol Rev* 2001;**81**:1031–64.
13. Wolever TM, Brighenti F, Royall D, Jenkins AL, Jenkins DJ. Effect of rectal infusion of short chain fatty acids in human subjects. *Am J Gastroenterol* 1989;**84**:1027–33.
14. Butzner JD, Parmar R, Bell CJ, Dalal V. Butyrate enema therapy stimulates mucosal repair in experimental colitis in the rat. *Gut* 1996;**38**:568–73.
15. Donohoe DR, Garge N, Zhang X, Sun W, O'Connell TM, Bunger MK, et al. The microbiome and butyrate regulate energy metabolism and autophagy in the mammalian colon. *Cell Metab* 2011;**13**:517–26.
16. Gao Z, Yin J, Zhang J, Ward RE, Martin RJ, Lefevre M, et al. Butyrate improves insulin sensitivity and increases energy expenditure in mice. *Diabetes* 2009;**58**:1509–17.
17. Canfora EE, Jocken JW, Blaak EE. Short-chain fatty acids in control of body weight and insulin sensitivity. *Nat Rev Endocrinol* 2015;**11**:577–91.
18. De Vadder F, Kovatcheva-Datchary P, Goncalves D, Vinera J, Zitoun C, Duchampt A, et al. Microbiota-generated metabolites promote metabolic benefits *via* gut–brain neural circuits. *Cell* 2014;**156**:84–96.
19. Furusawa Y, Obata Y, Fukuda S, Endo TA, Nakato G, Takahashi D, et al. Commensal microbe-derived butyrate induces the differentiation of colonic regulatory T cells. *Nature* 2013;**504**:446–50.
20. Gao Z, Zhang J, Henagan TM, Lee JH, Wang H, Ye X, et al. P65 inactivation in adipocytes and macrophages attenuates adipose inflammatory response in lean but not in obese mice. *Am J Physiol Endocrinol Metab* 2015;**308**:E496–505.
21. Yin J, Gao Z, Liu D, Liu Z, Ye J. Berberine improves glucose metabolism through induction of glycolysis. *Am J Physiol Endocrinol Metab* 2008;**294**:E148–56.
22. Ke B, Zhao Z, Ye X, Gao Z, Manganiello V, Wu B, et al. Inactivation of NF-κB p65 (RelA) in liver improved insulin sensitivity and inhibited cAMP/PKA pathway. *Diabetes* 2015;**64**:352–62.
23. Eckburg PB, Bik EM, Bernstein CN, Purdom E, Dethlefsen L, Sargent M, et al. Diversity of the human intestinal microbial flora. *Science* 2005;**308**:1635–8.

24. Zhang Y, Zhao Z, Ke B, Wan L, Wang H, Ye J. Induction of posttranslational modifications of mitochondrial proteins by ATP contributes to negative regulation of mitochondrial function. *PLoS One* 2016;**11**:e0150454.
25. Nøhr MK, Pedersen MH, Gille A, Egerod KL, Engelstoft MS, Husted AS, et al. GPR41/FFAR3 and GPR43/FFAR2 as cosensors for short-chain fatty acids in enteroendocrine cells *vs* FFAR3 in enteric neurons and FFAR2 in enteric leukocytes. *Endocrinology* 2013;**154**:3552–64.
26. Yadav H, Lee JH, Lloyd J, Walter P, Rane SG. Beneficial metabolic effects of a probiotic *via* butyrate-induced GLP-1 hormone secretion. *J Biol Chem* 2013;**288**:25088–97.
27. Ley RE, Backhed F, Turnbaugh P, Lozupone CA, Knight RD, Gordon JI. Obesity alters gut microbial ecology. *Proc Natl Acad Sci U S A* 2005;**102**:11070–5.
28. Zhang X, Zhao Y, Xu J, Xue Z, Zhang M, Pang X, et al. Modulation of gut microbiota by berberine and metformin during the treatment of high-fat diet-induced obesity in rats. *Sci Rep* 2015;**5**:14405.
29. Hao Z, Zhao Z, Berthoud HR, Ye J. Development and verification of a mouse model for Roux-en-Y gastric bypass surgery with a small gastric pouch. *PLoS One* 2013;**8**:e52922.
30. Ye J, Hao Z, Mumphrey MB, Townsend RL, Patterson LM, Stylopoulos N, et al. GLP-1 receptor signaling is not required for reduced body weight after RYGB in rodents. *Am J Physiol Regul Integr Comp Physiol* 2014;**306**:R352–62.
31. Lee JH, Zhang Y, Zhao Z, Ye X, Zhang X, Wang H, et al. Intracellular ATP in balance of pro- and anti-inflammatory cytokines in adipose tissue with and without tissue expansion. *Int J Obes* 2017;**41**:645–51.
32. Jin W, Cui B, Li P, Hua F, Lv X, Zhou J, et al. 1,25-Dihydroxyvitamin D3 protects obese rats from metabolic syndrome *via* promoting regulatory T cell-mediated resolution of inflammation. *Acta Pharm Sin B* 2018;**8**:178–87.
33. Liu Q, Liu S, Gao L, Sun S, Huan Y, Li C, et al. Anti-diabetic effects and mechanisms of action of a chinese herbal medicine preparation JQ-R *in vitro* and in diabetic kk^{Ay} mice. *Acta Pharm Sin B* 2017;**7**:461–9.
34. Holst JJ. The physiology of glucagon-like peptide 1. *Physiol Rev* 2007;**87**:1409–39.
35. Gniuli D, Calcagno A, Dalla Libera L, Calvani R, Leccesi L, Caristo ME, et al. High-fat feeding stimulates endocrine, glucose-dependent insulinotropic polypeptide (GIP)-expressing cell hyperplasia in the duodenum of wistar rats. *Diabetologia* 2010;**53**:2233–40.
36. Aranias T, Grosfeld A, Poitou C, Omar AA, Le Gall M, Miquel S, et al. Lipid-rich diet enhances L-cell density in obese subjects and in mice through improved L-cell differentiation. *J Nutr Sci* 2015;**4**:e22.
37. Dusaulcy R, Handgraaf S, Skarupelova S, Visentin F, Vesin C, Heddad-Masson M, et al. Functional and molecular adaptations of enteroendocrine L-cells in male obese mice are associated with preservation of pancreatic α-cell function and prevention of hyperglycemia. *Endocrinology* 2016;**157**:3832–43.
38. Sun Y, Jin C, Zhang X, Jia W, Le J, Ye J. Restoration of GLP-1 secretion by berberine is associated with protection of colon enterocytes from mitochondrial overheating in diet-induced obese mice. *Nutr Diabetes* 2018;**8**:53.
39. Wang W, Fang H, Groom L, Cheng A, Zhang W, Liu J, et al. Superoxide flashes in single mitochondria. *Cell* 2008;**134**:279–90.
40. Wang X, Zhang X, Wu D, Huang Z, Hou T, Jian C, et al. Mitochondrial flashes regulate ATP homeostasis in the heart. *eLife* 2017;**6**:e23908.
41. Duchen MR. Mitochondria and Ca^{2+} in cell physiology and pathophysiology. *Cell Calcium* 2000;**28**:339–48.
42. Chen WW, Birsoy K, Mihaylova MM, Snitkin H, Stasinski I, Yucel B, et al. Inhibition of ATPIF1 ameliorates severe mitochondrial respiratory chain dysfunction in mammalian cells. *Cell Rep* 2014;**7**:27–34.
43. Qin J, Li Y, Cai Z, Li S, Zhu J, Zhang F, et al. A metagenome-wide association study of gut microbiota in type 2 diabetes. *Nature* 2012;**490**:55–60.
44. Leng-Peschlow E. Dual effect of orally administered sennosides on large intestine transit and fluid absorption in the rat. *J Pharm Pharmacol* 1986;**38**:606–10.